3D CFD simulation of water droplet dynamics on a fuel cell Gas Diffusion Layer by considering a realistic woven structure

C. Antetomaso[a], S. S. Merola[b], A. Irimescu[c], B. M. Vaglieco[d], S. Di Micco[e] and E. Jannelli[f]

[a] CNR-STEMS, Naples, Italy, christian.antetomaso@stems.cnr.it
[a] University of Naples "Parthenope", Naples, Italy,
christian.antetomaso001@studenti.uniparthenope.it
[b] CNR-STEMS, Naples, Italy, simonasilvia.merola@stems.cnr.it
[c] CNR-STEMS, Naples, Italy, adrian.irimescu@stems.cnr.it
[d] CNR-STEMS, Naples, Italy, biancamaria.vaglieco@stems.cnr.it
[e] University of Naples "Parthenope", Naples, Italy, simona.dimicco@studenti.uniparthenope.it
[f] University of Naples "Parthenope", Naples, Italy, elio.jannelli@uniparthenope.it

Abstract:

Proton exchange membrane fuel cells have been identified as suitable for vehicle implementation. As for all fuel cell types, thermal management is a critical issue: the redox reactions taking place in the membrane electrode assembly generate water; a humid membrane is able to enhance transport phenomena, but too much water could flood the pathways of reactant gases. Recently, interest has grown with respect to the properties of the gas diffusion layer of membranes: its fibres pattern can critically affect water removal rates. Computation fluid dynamics represents a powerful tool that can be used for understanding the key design factors of fuel cell components to improve the overall performance. Specifically, in the case of the diffusion layer, 3D simulation can investigate droplet dynamics and define the optimized surface structure for water management. In this paper, optical data and numerical results were combined to characterize the behaviour (oscillation, detachment, etc) of a couple of droplets on the woven gas diffusion layer with a structure retrieved by using an approach typical of the textile industry. High-spatial resolution imaging allowed the evaluation of warp/weft size; these parameters were used for building the 3D mesh for simulations based on the Volume of fluid method. The dynamics of droplets, with diameters ranging from 200 to 600 μm, were investigated under the effect of a constant 10 m/s airflow for different gas diffusion layer geometries. In addition, the cases of the droplet pairs, deposited at different reciprocal distances, were studied by using the same methodological approach. Results demonstrated the impact of layer structure on the results obtained through simulations; moreover, an optimised design can contribute to control water removal and minimise flooding effects.

Keywords:

3D CFD, optical visualization, water dynamics, gas diffusion layer

1. Introduction

Among the numerous types of fuel cells, Proton Exchange Membrane (PEM) Fuel Cells (FCs) have gained a lot of interest in automotive industries due to the absence of pollutant emissions from the end gases pipeline and its low operative temperature. PEM FC is an established and reliable technology, but it still presents unresolved issues. Among them, water management is one of the most critical, given the need to humidify the membrane and the simultaneous risk of flooding the reactant pathways toward the catalyst layer.

In the last decade, research activities regarding water dynamics in PEM FCs were mainly focused on the design and characteristics of bipolar plates [1]: fabrication methods and innovative materials, suitable coatings and efficient channel design to simultaneously improve reactants diffusion and water removal rate. Those were the routes to further develop PEM FCs. Only recently, the design of properties of cloth Gas Diffusion Layer (GDL) have been considered more carefully [2], with the aim of improving water management by means of a potentially controlled droplet adhesion on the surface, while also studying flow through GDL. In this regard, efforts were mainly directed toward a deep comprehension on how the number and the pores dimension [3], fibers radius and distribution [4], porosity and permeability [5-6] and interface between GDL

and Catalyst Layer (CL) [7-8] can improve the FCs overall performances: optimization of the design of this layer is fundamental since GDL serves both as pathway for reactant gases and escape route for the forming water. However, as water emerge from GDL, is also important to boost its removal rate. Thus, starting from the well-known concept that the GDL wettability and surface roughness affect water dynamics [9-10], specific solutions such as GDL perforation [11] characteristics have been studied to enhance the drainage of the water from the electrode to the gas channel and to reduce the risk of flooding. As concern the numerical simulation of water detachment/rolling/sliding, both the lattice Boltzmann and the Volume Of Fluid (VOF) methods have been widely used to investigate droplet behaviour on the GDL with different channel geometry. A common assumption made in these models is to consider a smooth GDL surface [12-13], but recently authors started to investigate the role that microgeometry may play in membrane optimal design. Hou et. Al [14] used the lattice Boltzmann method to simulate droplet motion on a realistic GDL, confirming that a smooth surface led to faster water removal. Liu et al. [15] performed a 3D VOF assuming different patterns for the GDL: it was still an impermeable and hydrophobic surface, but they used a striped, dotted and waved surface to study the effects of GDL's microstructure and optimize the shape parameters of those "disturbances". Anyanwu et al. [16] compared the liquid water transport in wave-like channels for smooth and rough GDL. They substantially demonstrated that smaller fiber diameters and more ordered and uniform microstructure reduced the flooding of flow channels by favouring water removal. Wang et al. [10] performed molecular simulation of a droplet and proposed to improve water removal capacity by controlling superficial roughness of the GDL. Gao et. Al [4] focused their effort on reconstructing a realistic microgeometry for the outer layer of the Membrane Electrode Assembly (MEA) and evaluated the fluid flow through it. The nature of the woven structure allowed them to define a primitive cell: the interlaced GDL was represented by serial repetition of this primitive element.

Currently, few research efforts have combined experimental results and simulation analysis related to the droplet movement on a real GDL surface. In this paper, optical data and numerical results were combined to characterize the behaviour (oscillation, detachment, etc) of droplets on the woven GDL with a structure retrieved by using a typical approach of the textile industry. High-spatial resolution imaging allowed the evaluation of warp/weft size; these parameters were used for building the 3D mesh for CFD simulations based on the VOF method. The single droplets and pairs, with diameters ranging from 200 to 600 μm, were deposited at different reciprocal distances and their dynamics were studied under the effect of a constant 10 m/s airflow. Results obtained by simulations with different microstructure geometries were compared. In particular, a completely smooth surface and a hybrid one between the previous two were generated.

2. Experimental setup

Water dynamics were studied on the carbon cloth GDL of a Celtec®-P1000 membrane electrode assembly (MEA) with an active area of 45 cm^2 (6.72 by 6.72 cm). In order to support the CFD simulations, optical methodologies were applied to determine the structure of the GDL and the static contact angles of deposited water droplets. The GDL texture and profile were visualised by means of an 8-LED ring crown illuminator mounted on a 1280x720 digital microscope (Technaxx TX-158). This was equipped with a 1000x digital zoom system that permitted to range the spatial resolution up to 5.8 μm/pixel in full chip configuration. In Fig.1a-b, the texture with woven fibres is clearly distinguishable. Following an approach derived from the textile industry [17-18], a custom routine for image processing was developed by using NI Vision [19]; it allowed delineating the GDL geometrical cross-section (Fig.1c).

(a)

(b)

(c)
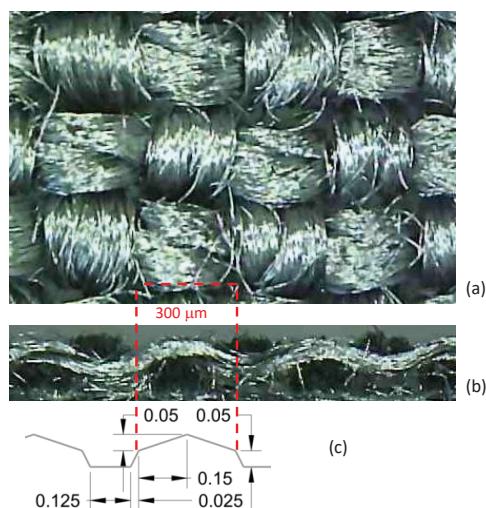
Figure. 1. GDL carbon cloth texture: (a) experimentally visualised surface and (b) profile; (c) geometrical profile used for CFD simulations (units are expressed in µm).

The GDL surface was mapped in 25 regions of interest 1x1 cm in size (Fig. 2a). On each region, a stainless-steel needle of a high-precision medical device (NIPRO) was used for depositing several droplets with a minimum diameter of 400 µm (due to the internal dimension of the capillary) [19-20]. With the digital visualization set-up described previously, droplet morphology was evaluated in terms of diameter and static contact angle. The occurrence distribution related to 115 droplets (Fig. 2b) demonstrated that the most probable contact angle (CA) for droplet in the 400-800 µm size range was 123±2 deg. This value agreed with those considered by other researchers for woven GDL surfaces [21]. The measured contact angles were practically constant, as shown in Fig. 3 that reports the average values measured for 9 classes of droplet diameters (from 400 µm to 800 µm step 50 µm). Consequently, 123 deg was used as boundary condition for the wettability parameter in the CFD simulations.

(a)   (b)
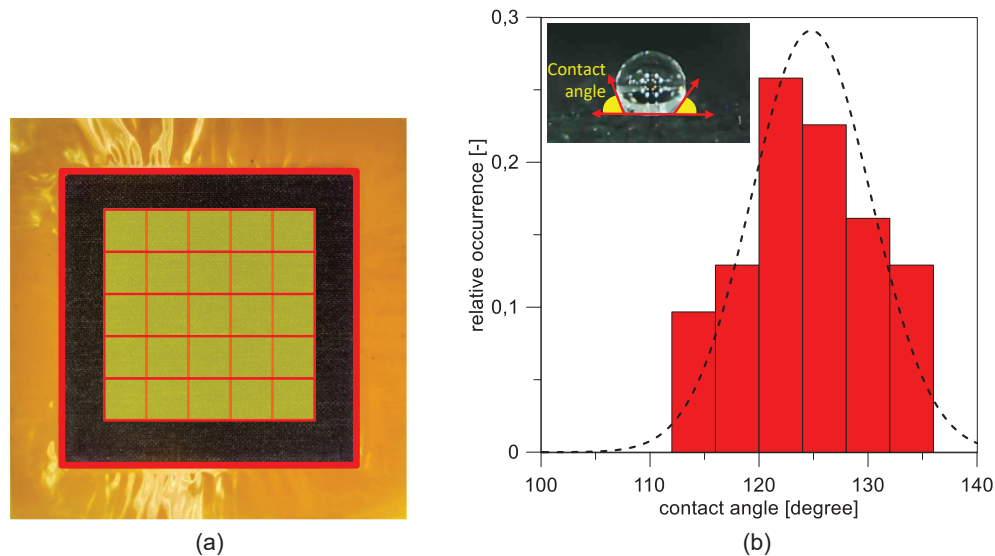
Figure. 2. (a) MEA with 25 regions of interest highlighted on GDL surface for optical investigations and (b) occurrence distribution of droplet contact angles.
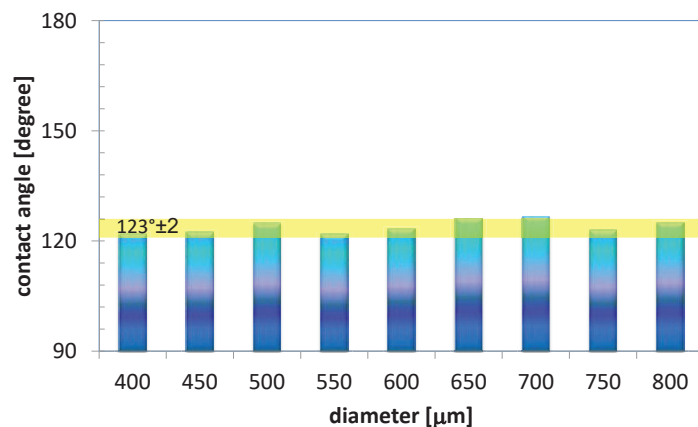
Figure. 3. Average contact angle of 9 classes of droplet diameter.

Droplet dynamics were investigated by using a 512x512 CMOS camera (5000fps in full chip configuration) coupled with a 25 mm objective. The setup allowed to achieve a spatial resolution of 55 µm/pixel. The exposure time was fixed in order to detect 1000 images per second; the setting represented a good compromise between luminosity and temporal resolution. Another image processing procedure developed

using NI Vision 2020 was applied for assessing the instantaneous contour and the centre of mass of the droplets. For dynamic conditions, 10m/s airflow was provided by a fan positioned at 50 mm from the region of droplet deposition; local air velocity was measured with an accuracy of 0.1 m/s by using a hot-film probe.

Optical investigations were performed in open-channel conditions. Since the air-flow rate and static wettability were fixed, the surface roughness was the only parameter that influenced the dynamic wettability and the adhesive force at the liquid-solid interface. In real-working configuration, humidity of the reactant gas should be considered when evaluating the removal efficacy of droplets from the GDL and flow channel. This is due to the fact that phase change phenomena and modifications in surface tension could occur. Nevertheless, this study mainly focused on the effects of airflow and GDL roughness on droplet removal; the effects of reactant gas humidity was out of the scope of the present work, but will be considered in future investigations.

3. Methodology

3.1. GDLs design

Taking into account the GDL's microstructural characteristics determined by optical methodologies, CREO Parametric 8.0 was used to design the 3D profile. The optical analysis was able to recover the two key parameters to reconstruct a realistic geometry: the height and length of the sinusoidal waves that interlaces on the surface. These dimensions, together with the width of the weft, were used to trace four sweep trajectories for a trapezoidal profile. The four surfaces were then merged and trimmed to obtain a squared elemental region. The latter could be used in the "Serial Repetition" CREO function to create a surface of the desired dimensions. Figure 4 shows the generation process and the obtained elemental region. Two more GDL surfaces were generated: a completely smooth and a hybrid solution one. The generation of the latter follow the same methodology showed in Figure 4, but amplitude and length were set equal to 0.075 mm and 0.4 mm respectively.
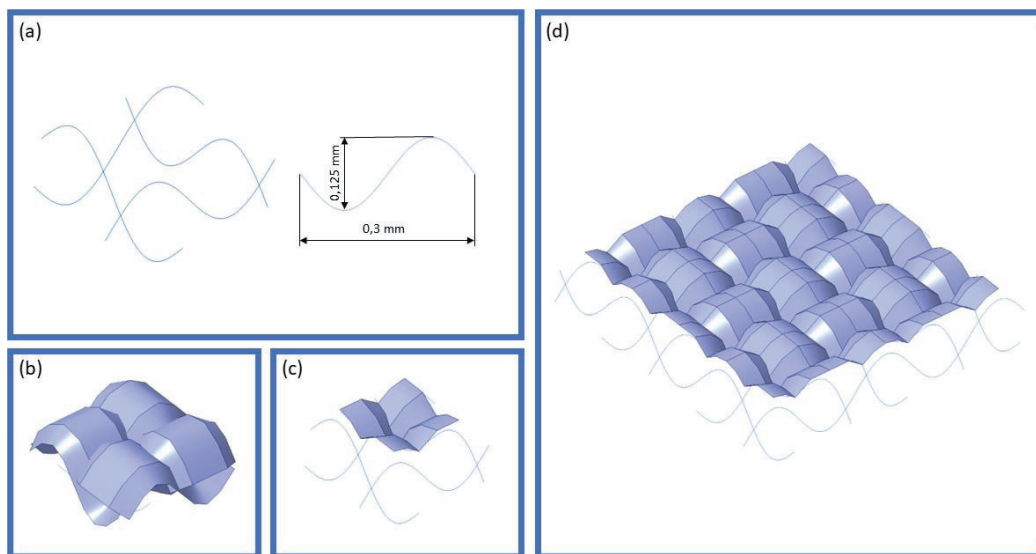
Figure. 4. Steps followed in generating the realistic GDL: (a) definition of 4 sinusoidal waves and their dimensions; (b) sweep of a trapezoidal profile on the defined trajectories; (c) surface trimming and identification of elemental regions; (d) serial repetition of elemental regions.

3.2. Governing equations

The VOF is one of the most used methods to simulate multiphase flow and it is the one adopted in this paper. The main characteristic of this method is that it assigns a numerical value to each cell. This index α_q represent the fraction of secondary phase presents in the cell; in particular:

- $\alpha_q = 0$, the cell contains pure primary phase,

- α_q = 1, the cell contains pure secondary phase,
- $0 < \alpha_q < 1$, the cell contains a mixture of the two phases,

given that:

$$\sum_{q=1}^{n} \alpha_q = 1 \tag{1}$$

For every cell, with n equals to the number of phases in the flow. Considering two phases (air and liquid water), viscosity μ and density ρ are evaluated through a weighted mean as shown in Formula (2) and (3).

$$\rho = (1 - \alpha) \cdot \rho_1 + \alpha \cdot \rho_2 \tag{2}$$

$$\mu = (1 - \alpha) \cdot \mu_1 + \alpha \cdot \mu_2 \tag{3}$$

Mass conservation is expressed as:

$$\frac{\partial \rho}{\partial t} + \nabla(\rho \cdot \overline{v}) = 0 \tag{4}$$

A single momentum equation is solved through the domain:

$$\frac{\partial}{\partial t}(\rho \cdot \overline{v}) + \nabla(\rho \cdot \overline{v} \cdot \overline{v}) = -\nabla p + \nabla\left[\mu\left(\nabla\overline{v} + \nabla\overline{v}^T\right)\right] + \rho \cdot \overline{g} + \overline{F} \tag{5}$$

The Continuum Surface Force (CSF) model for a two-phase flow can be simplified as:

$$\overline{F} = \sigma \cdot \frac{\rho \cdot k \cdot \nabla \alpha}{\frac{1}{2} \cdot (\rho_1 + \rho_2)} \tag{6}$$

where σ and k are surface tension coefficient and surface curvature of the interface respectively.

3.3. Domain definition and simulation setup

The elemental square previously defined was used to model one of the surfaces of a 1x1x4.8 mm box and to obtain the simulation domain. The modified surface would represent the hydrophobic and impermeable GDL, whilst the others would represent the velocity inlet, pressure outlet and channel walls. The base dimension of the cell was set to 0.02 mm. A three layers inflation was added on the GDL.

Simulations were performed with Ansys Fluent 2022 R1. The whole domain was initialized as still air, then a water droplet was deposited on the GDL surface at 1 mm distance from the velocity inlet. Droplets ranged from 200 to 600 μm. From 0 to 1 ms of simulation, the inlet would be set to 0 m/s to allow the droplet to properly set on the surface. Thereafter a constant airflow of 10 m/s started to push the droplet. The flow was assumed to be laminar. Surface tension coefficient between water and air was set to 0.072 N/m and wall adhesion model was enabled.

The pressure-based solver was used for transient 3D simulation. Pressure-Implicit with Splitting of Operators (PISO) algorithm was selected for pressure-velocity coupling. PREssure STaggering Option (PRESTO!), Second Order Upwind and Geo-Reconstruct schemes were used respectively for pressure, momentum and volume fraction. Adaptive multiphase specific time step was adopted to improve solution stability. Simulated time was set to 25 ms.

4. Results and discussions

The typical liquid drainage process inside a GDL flow channel includes droplets emerging, growing, detachment, and removal. After the detachment, the airflow drives the liquid droplet out of the channel and another droplet emerges from the GDL pore simultaneously [13]. Water removal is mainly realized according three modes of movement: rolling, lifting, and break-up [22]. Studies demonstrated that the occurrence of each mode was influenced by the airflow rate, while no definitive results on the effects of surface roughness were discussed [23]. The first case in which it is possible to immediately identify the importance of a realistic interlaced GDL surface is the one that features 300 μm droplet diameter. Figure 5 clearly shows how the droplets on the realistic and hybrid surface were able to reach the exit of the closed channel, but with a significant time difference with respect to the flat design.

Dimensions of pores between warp and weft yarns of GDL texture comparable with the droplet diameter led to a longer detachment phase and slower movement towards the outlet. Figure 6 shows that at increasing droplet size the GDL microstructure decreased its influence on the water removal process; 600 μm droplets moved out the channel domain almost simultaneously for the realistic and hybrid case. For a more detailed characterization of droplet dynamics, high-speed visualization was applied for diameters of 600±20 μm as

estimated in static conditions. Fig.7a reports several selected frames of a 50ms sequence recorded for a 605 μm droplet. In agreement with the literature [24], after liquid deposition (#1) switching-on the fan determined around 1 second of droplet contour oscillations (as shown in frames #2-#3) due the balance between detaching and retention forces [25-26]. This occurred until a critical local velocity was reached; then the droplet started to move in the direction of the air-flow (#4) and reached the limit of the optical region in about 6 ms. It should be noted that the droplet motion was characterised by rolling rather than sliding. Thus the assumption to fix the GDL wettability without differentiating between advancing and receding angles resulted reasonable.
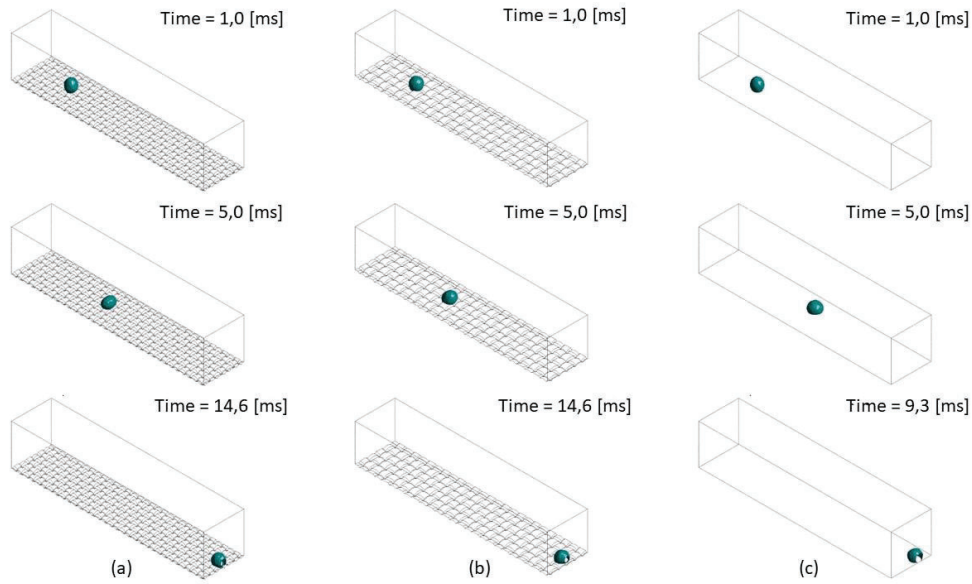
Figure. 5. Water fraction isosurface (equal to 0.8) for different GDLs for a 300 μm droplet. (a) Realistic GDL, (b) Hybrid GDL, (c) Flat channel surface.
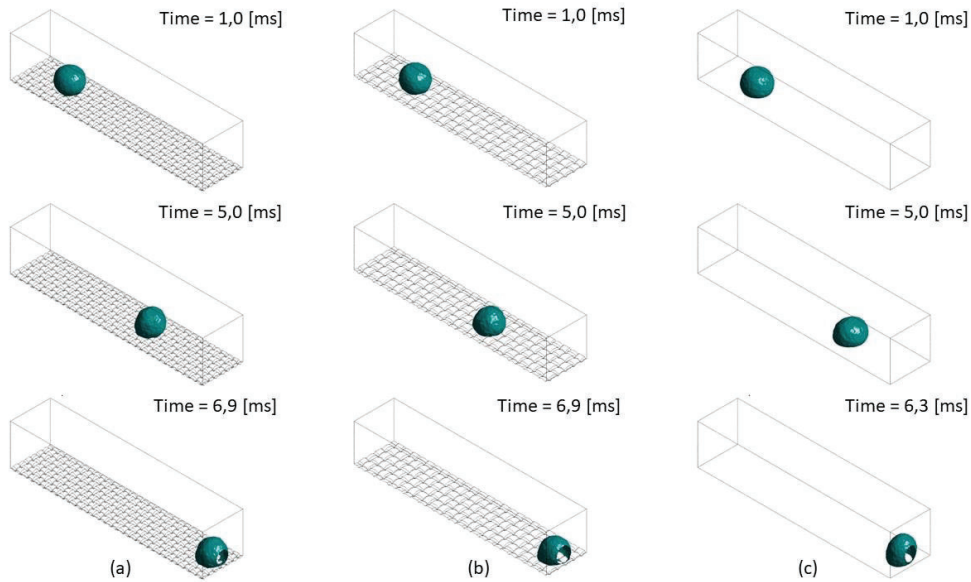
Figure. 6. Water fraction isosurface (equal to 0.8) for different GDLs for a 600 μm droplet. (a) Realistic GDL, (b) Hybrid GDL, (c) Flat channel surface.

The optical data were used for validating the simulation results; Fig.7b shows the comparison between the temporal evolution of the distance from the deposition point along the air-flow direction of a 600 μm droplet. The experimental results show the average value of the luminous center of mass calculated based on 15 sequences. The error bars correspond to the standard deviation. The agreement between simulation and experiments is very good; the discrepancy observed after 5 ms was due to the open channel condition of the optical tests that determined lower pressure forces on the droplet and thus lower acceleration. Nonetheless, it can be stated that model validation is satisfactory.
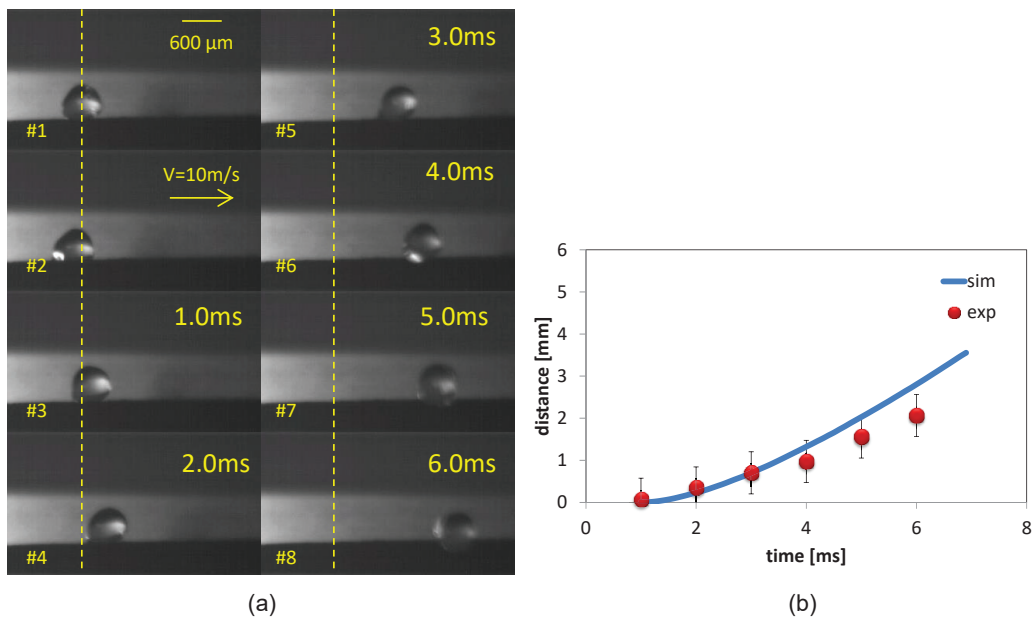
Figure. 7. Visualization of the droplet motion on the GDL (a) and comparison with simulation results (b).
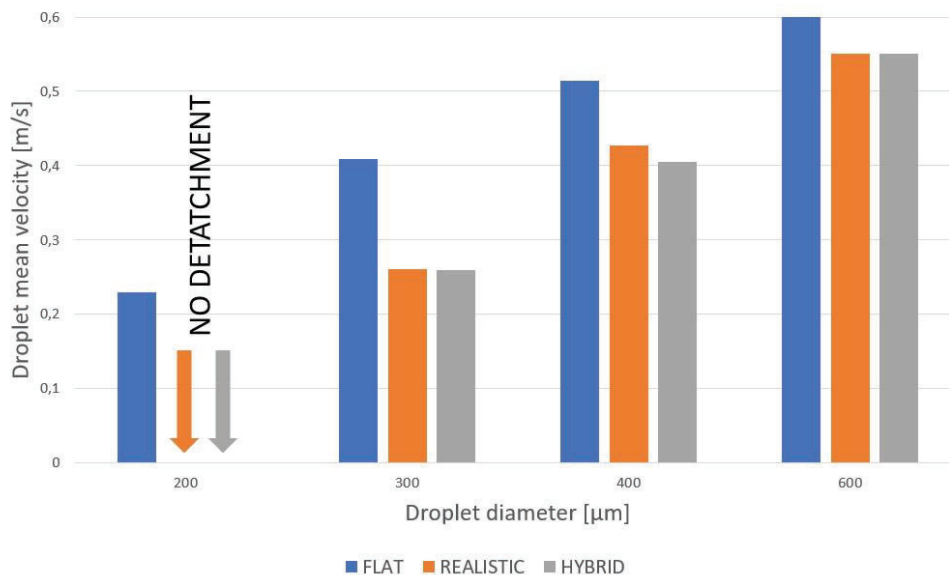
Figure. 8. Comparison of droplet mean velocity for all dimensions and cases analysed.

Fig.8 shows the mean droplet velocity for all the analyzed cases. Once again, the graph remarks that the importance of GDL microstructure is noticeably higher for smaller dimension, when droplet and pores have comparable sizes. However, even in the 600 μm case the droplet mean velocity is around 8% lower for the realistic and hybrid case, so still a significant amount.

Initial water removal time was defined as the instant in which the droplet as a whole surpassed a plane perpendicular to the airflow and passing through the middle of the drop when it is deposited. Figure 9 shows simulations results. For sure the flat surface is the one that led to faster removal since there are no obstacles in the way of the droplet. On the other hand, the pores of the realistic and hybrid surfaces offer a certain resistance to the initial rolling of the droplet. Moreover, even though the hybrid case has a lower sinusoidal amplitude and a higher wavelength and thus should be more similar to the flat one, it seems to offer more initial resistance. This outcome is linked to the fact that it also has a bigger wet area with respect to the realistic surface, increasing the adhesive force. These results agree with literature [14-15] that found that the GDL microstructure can slow down the droplet motion compared to the smooth surface simplification.

It worth noting that for both Fig. 8 and Fig. 9 the leftmost column reports a "no detachment" condition for the 200 μm case, since the droplet get stuck in membrane pores. This is a critical condition for the FC operation, since those droplets decrease overall efficiency by:

▪ blocking reactants flux towards the CL causing flooding and thus cell starvation.

▪ shielding the incoming airflow, thus reducing water removal rate for downstream drops; as distance increases, airflow reattach to GDL and this effect is reduced.

Water keeps on forming in the CL and the droplet will reach critical dimension and finally be removed. In this sense, the design of GDL superficial microgeometry determines critical detachment diameter.

1022
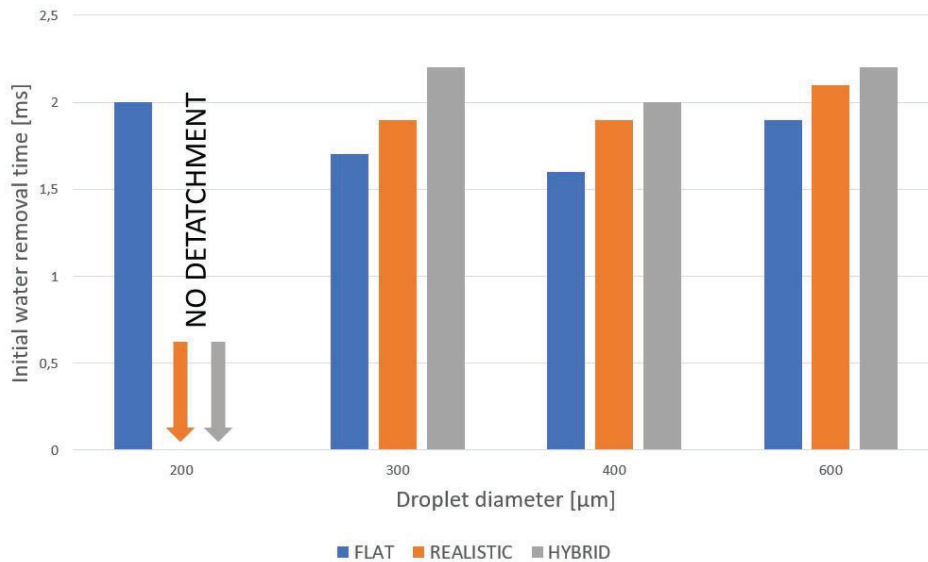
Figure. 9. Confront on droplet initial water removal time for all dimensions and cases analysed

The following step was to investigate how a second droplet could influence the behaviour of the first one. With this purpose, another set of simulation was prepared: a 300 μm droplet was deposited in the same position of the single case (1 mm from the inlet, middle of the channel), and a second one was initialized further in the channel, at a distance that depended on GDL microgeometry. For the real and the hybrid case, the second droplet was deposited in the fourth pore after the first droplet. Figure 10 graphically shows the used principle. For the flat case the used distance was the mean of the distances for the two other cases.
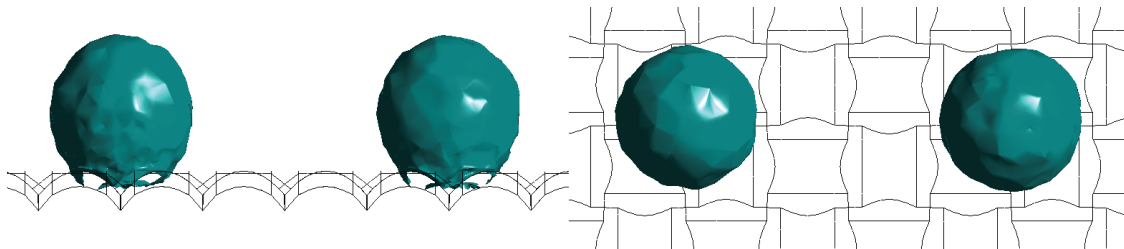
Figure. 10. Reciprocal positioning of the two droplets on the GDL

Simulated droplets at different time steps are shown in Figure 11. Once again, the effect of microgeometry design is highlighted by the difference in flat-realistic cases and realistic-hybrid one. As already seen for the single droplet case, the flat surface offers minimal resistance to the rolling of the pair, however the first droplet partially shield the second one from the incoming airflow, thus it moves at an higher speed. Moreover, the lower the distance between the two droplets, the higher seems to become the speed difference. A parametrization of droplet pair diameters and distances could be of interest for future study. As concern the realistic case, a similar behaviour was observed, but the mean velocities are lower and the initial detachment phase is longer. The comparison of realistic and hybrid case remarked the importance of GDL microstructure: in the hybrid case the second droplet was stuck in position due to the shielding of the first one and the higher wet area with respect to the realistic one. The hybrid GDL showed the highest exit time for this set of simulations.

https://doi.org/10.52202/069564-0092
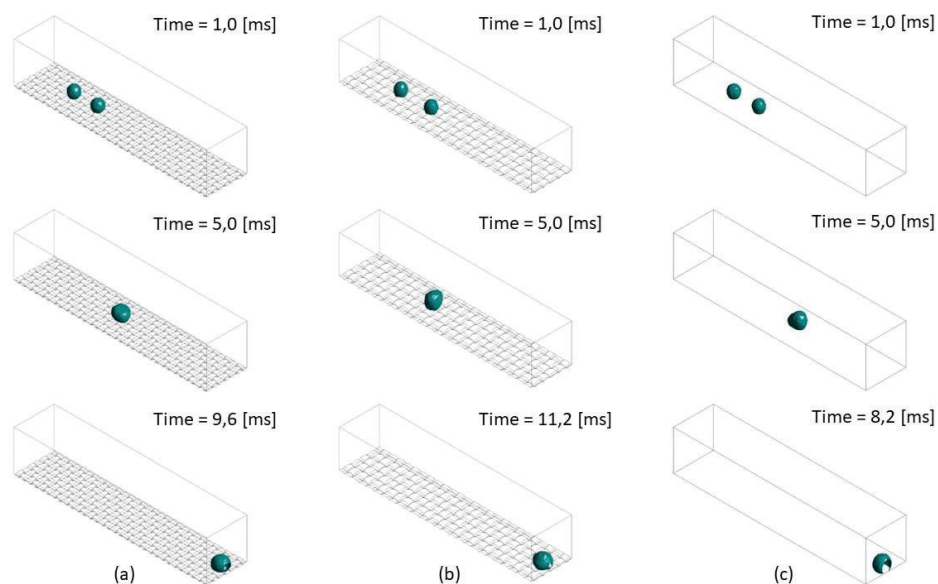
Figure. 11. Water fraction isosurface (equal to 0.8) for different GDLs for the 300-300 μm droplets pair. (a) Realistic GDL, (b) Hybrid GDL, (c) flat GDL

5. Conclusions

PEM FCs represent a decisive step in the direction of a cleaner mobility, but it is a device still far from optimal operation conditions. Experimental and simulation studies are fundamental to fully develop the technology, and in realizing models able to reproduce the actual behaviour of a cell it is important not to over-model a phenomenon. The surface microgeometry of a fuel cell is often deemed as negligible in channel flow simulations. The aim of this study has been to evaluate the importance of this microgeometry and to state if it should be taken into consideration when accounting for water removal rate of a cell.

The main results of this study can be summarized as follow:

- The importance of pores on the surfaces rises as smaller droplets are considered. Starting from the same initial and boundary conditions, the 200 μm droplet on the flat surface was able to reach the outlet, whilst for the others GDLs the drop was stuck in the pore. The influence of the surface is lower for bigger droplet, however even for the 600 μm droplet the mean velocity difference is around 8%.

- The microstructure also affects the initial water removal time of the droplet. The flat surface is the one that shows lower removal time, whilst the other two structures seem to slow down this phenomenon due to the presence of pores that work as obstacles for the droplet. In particular, the hybrid case is the slowest one, due to the fact that it has a bigger wet area with respect to the realistic surface, increasing the adhesive force.

- Simulations showed the influence of a second droplet deposition on different GDLs. Flat surface offers the highest water removal rate, while realistic and hybrid cases shows a behaviour linked to microgeometry design. In particular, due to the partial shielding effect and the higher wet area of the hybrid surface, the second droplet resulted stuck in the pore until it merged with the first one.

Next steps of the reported activity are planned for further improving the water dynamic modelling and evaluate the weight of commonly used approximations on predictive simulations. Specifically, the GDL intrusion in the gas channel and surface deformation near the channel ribs due to the clamping pressure of the cell will be estimated for a more realistic design. Moreover, the reactant gas humidity in closed channel configurations will be considered in the model. These parametric studies are on-going to further shed light on the possibility of a design for promoting controlled water removal mechanisms.

Acronyms

CA	Contact angle
CL	Catalyst Layer
CSF	Continuum Surface Force
FC	Fuel Cell

GDL   Gas Diffusion Layer
MEA   Membrane Electrode Assembly
PEM   Proton Exchange Membrane
VOF   Volume Of Fluid

References

[1] Y. Song, C. Zhang, C. Y. Ling, M. Han, R. Y. Yong, D. Sun, J. Chen, Review on current research of materials, fabrication and application for bipolar plate in proton exchange membrane fuel cell. *International Journal of Hydrogen Energy*, 2020, *45*(54), 29832-29847, https://doi.org/10.1016/j.ijhydene.2019.07.231

[2] G. Athanasaki, A. Jayakumar, A. M. Kannan, Gas diffusion layers for PEM fuel cells: Materials, properties and manufacturing–A review. *International Journal of Hydrogen Energy*, 2022, *48*(6), 2294-2313, https://doi.org/10.1016/j.ijhydene.2022.10.058

[3] J. Cho, H. Oh, J. Park, K. Min, E. Lee, J. Y. Jyoung, Study on the performance of a proton exchange membrane fuel cell related to the structure design of a gas diffusion layer substrate. *International journal of hydrogen energy*, 2014, *39*(1), 495-504, http://dx.doi.org/10.1016/j.ijhydene.2013.10.057

[4] Y. Gao, T. Jin, X. Wu, Stochastic 3D carbon cloth GDL reconstruction and transport prediction. *Energies*, 2020, *13*(3), 572, https://doi.org/10.3390/en13030572

[5] B. P. Abraham, K. K. Murugavel, Influence of catalyst layer and gas diffusion layer porosity in proton exchange membrane fuel cell performance. *Electrochimica Acta*, 2021, *389*, https://doi.org/10.1016/j.electacta.2021.138793

[6] H. Pourrahmani, J. Van herle, Water management of the proton exchange membrane fuel cells: Optimizing the effect of microstructural properties on the gas diffusion layer liquid removal. *Energy*, 2020, *256*, 124712, https://doi.org/10.1016/j.energy.2022.124712

[7] Y. Hiramitsu, K. Kobayashi, M. Hori, Gas diffusion layer design focusing on the structure of the contact face with catalyst layer against water flooding in polymer electrolyte fuel cell. *Journal of Power Sources*, 2010, *195*(22), 7559-7567, https://doi.org/10.1016/j.jpowsour.2010.05.067

[8] L. Guo, L. Chen, R. Zhang, M. Peng, W. Q. Tao, Pore-scale simulation of two-phase flow and oxygen reactive transport in gas diffusion layer of proton exchange membrane fuel cells: Effects of nonuniform wettability and porosity. *Energy*, 2022, *253*, 124101, https://doi.org/10.1016/j.energy.2022.124101

[9] Y. Wang, T. Liu, H. Sun, M. Yao, S. Liu, Y. Qin, X. Wang, Droplet dynamic behaviors on gas diffusion layer surface of various wettabilities in a PEMFC gas flow channel. *International Journal of Green Energy*, 2021, *18*(13), 1369-1382, https://doi.org/10.1080/15435075.2021.1904940

[10] X. L. Wang, W. K. Wang, Z. G. Qu, G. F. Ren, H. C. Wang, Surface roughness dominated wettability of carbon fiber in gas diffusion layer materials revealed by molecular dynamics simulations. *International Journal of Hydrogen Energy*, 2021, *46*(52), 26489-26498, https://doi.org/10.1016/j.ijhydene.2021.05.121

[11] D. Gerteisen, T. Heilmann, C. Ziegler, Enhancing liquid water transport by laser perforation of a GDL in a PEM fuel cell. *Journal of Power Sources*, 2008, *177*(2), 348-354, https://doi.org/10.1016/j.jpowsour.2007.11.080

[12] M. Andersson, A. Mularczyk, A. Lamibrac, S. B. Beale, J. Eller, W. Lehnert, F. N. Büchi, Modeling and synchrotron imaging of droplet detachment in gas channels of polymer electrolyte fuel cells. *Journal of power sources*, 2018, *404*, 159-171, https://doi.org/10.1016/j.jpowsour.2018.10.021

[13] R. Chen, Y. Qin, S. Ma, Q. Du, Numerical simulation of liquid water emerging and transport in the flow channel of PEMFC using the volume of fluid method. *International Journal of Hydrogen Energy*, 2020, *45*(54), 29861-29873, https://doi.org/10.1016/j.ijhydene.2019.07.169

[14] Y. Hou, H. Deng, N. Zamel, Q. Du, K. Jiao, 3D lattice Boltzmann modeling of droplet motion in PEM fuel cell channel with realistic GDL microstructure and fluid properties. *International Journal of Hydrogen Energy*, 2020, *45*(22), 12476-12488, https://doi.org/10.1016/j.ijhydene.2020.02.155

[15] S. Liu, L. Zhang, Z. Wang, R. Li, Influence of the surface microstructure of the fuel cell gas diffusion layer on the removal of liquid water. *International Journal of Hydrogen Energy*, 2021, *46*(62), 31764-31777, https://doi.org/10.1016/j.ijhydene.2021.07.051

[16] I. S. Anyanwu, Z. Niu, D. Jiao, A. U. H. Najmi, Z. Liu, K. Jiao, Liquid water transport behavior at GDL-channel interface of a wave-like channel. *Energies*, 2020, *13*(11), 2726, https://doi.org/10.3390/en13112726

[17] M. M. B. Hasan, A. Calvimontes, A. Synytska, V. Dutschk, Effects of topographic structure on wettability of differently woven fabrics. *Textile Research Journal*, 2008, *78*(11), 996-1003, https://doi.org/10.5772/10477

[18] A. Calvimontes, V. Dutschk, M. Stamm, Advances in topographic characterization of textile materials. *Textile research journal*, 2010,*80*(11), 1004-1015, https://doi.org/10.1177/0040517509348331

[19] C. Antetomaso, A. Irimescu, S. S. Merola, B. M. Vaglieco, S. Di Micco, E. Jannelli, G. Scarpati, E. Simeoni, CFD simulation of water droplet adhesion on the GDL of a low temperature PEM FC in air cross-flow conditions. ATI 2022 proceeding, 2022 Sep 12-14, published in *Journal of Physics: Conference Series*, 2385(1), 12074, https://doi.org/10.1088/1742-6596/2385/1/012074

[20] C. Antetomaso, S. S. Merola, A. Irimescu, B. M. Vaglieco, S. Di Micco, E. Jannelli, G. Scarpati, E. Simeoni, CFD simulation of the interaction between water droplets on the GDL of a low temperature PEM FC in conditions of air cross-flow, EAEC 2022 proceeding, 2022 Oct 26-28.

[21] Y. D. Wang, Q. Meyer, K. Tang, J. E. McClure, R. T. White, S. T. Kelly, M. M. Crawford, F. Iacoviello, D. J. L. Brett, P. R. Shearing, P. Mostaghimi, C. Zhao, R. T. Armstrong, Large-scale physically accurate modelling of real proton exchange membrane fuel cell with deep learning. Nature Communications, 2023, 14(1), 745. https://doi.org/10.1038/s41467-023-35973-8

[22] S. Xu, P. Liao, D. Yang, Z. Li, B. Li, P. Ming, X. Zhou, Liquid water transport in gas flow channels of PEMFCs: A review on numerical simulations and visualization experiments. *International Journal of Hydrogen Energy*, 2023, 48(27), 10118-10143, https://doi.org/10.1016/j.ijhydene.2022.12.140

[23] M. Li, Y. Li, Y. Qin, Y. Yin, J. Zhang, Z. Che, Water droplet detachment characteristics on surfaces of gas diffusion layers in PEMFCs. *International Journal of Hydrogen Energy*, 2022, *47*(18), 10341-10351, https://doi.org/10.1016/j.ijhydene.2022.01.077

[24] S. Burgmann, M. Dues, B. Barwari, J. Steinbock, L. Büttner, J. Czarske, U. Janoske, Flow measurements in the wake of an adhering and oscillating droplet using laser-Doppler velocity profile sensor. *Experiments in Fluids*, 2021, *62*, 1-16, https://doi.org/10.1007/s00348-021-03148-0

[25] A. Esposito, A. D. Montello, Y. G. Guezennec, C. Pianese, Experimental investigation of water droplet–air flow interaction in a non-reacting PEM fuel cell channel. *Journal of Power Sources*, 2010, *195*(9), 2691-2699, https://doi.org/10.1016/j.jpowsour.2009.11.078

[26] S. Burgmann, V. Krämer, M. Rohde, M. Dues, U. Janoske, Inner and outer flow of an adhering droplet in shear flow. *International Journal of Multiphase Flow*, 2022, *153*, 104140, https://doi.org/10.1016/j.ijmultiphaseflow.2022.104140